

# Quasinormal-modes of the Kerr-Newman black hole: GW150914 and fundamental physics implications

Hai-Tian Wang,<sup>1,2</sup> Shao-Peng Tang,<sup>1,2</sup> Peng-Cheng Li,<sup>3,4,\*</sup> and Yi-Zhong Fan<sup>1,2</sup>

<sup>1</sup>*Purple Mountain Observatory, Chinese Academy of Sciences, Nanjing 210023, P.R. China*

<sup>2</sup>*School of Astronomy and Space Science, University of Science and Technology of China, Hefei, Anhui 230026, P.R. China*

<sup>3</sup>*Center for High Energy Physics, Peking University,*

*No.5 Yiheyuan Rd, Beijing 100871, P. R. China*

<sup>4</sup>*Department of Physics and State Key Laboratory of Nuclear Physics and Technology, Peking University, No.5 Yiheyuan Rd, Beijing 100871, P.R. China*

(Dated: April 16, 2021)

We develop an analytical approach, verified by the nice agreement with the numerical relativity simulation results, to calculate the quasinormal mode spectrum of the Kerr-Newman black hole. Then we analyze the gravitational wave data with the ringdown waveform model including both the fundamental mode and the overtone modes, and find that it can efficiently constrain the charge of the source. For GW150914, the charge-to-mass ratio of the remnant black hole is constrained to be  $\leq 0.38$  at 90% credibility. Our waveform model can be widely applied to other GW150914 like events. With the sole ringdown data, it is capable of constraining the electric, magnetic, or other  $U(1)$  dark charges carried by black holes, as well as the deviation parameter ( $\alpha$ ) of the scalar-tensor-vector gravity. Indeed, a constraint of  $\alpha \leq 0.17$  is achieved with the ringdown data alone for the first time.

## I. INTRODUCTION

A single distorted black hole (BH) is formed after the violent plunge of compact binary black hole (BBH). The gravitational wave (GW) radiation in this stage is called ringdown until it settles to a stationary state. The ringdown spectrum is described by superposition of quasinormal modes (QNMs), in the form of damped sinusoids [1–3]. These damped sinusoids are determined by the “hairs” of the final BH. According to general relativity (GR), the properties of a BH can be fully described by its mass  $M$ , dimensionless spin  $\chi$ , and charge-to-mass ratio  $\lambda$  [4–7]. The astrophysical BHs are widely believed to be uncharged since the interaction with surrounding non-electric neutral environment could quickly neutralize the charge, if there was. However, up to now unequivocally observational evidence for the neutrality of BH is still lacking. The existing constraints from the electromagnetic (EM) observations are model-dependent [8, 9]. Besides, in the minicharged dark matter model, charged BH could be formed in the early universe and will not be neutralised by accreting dark matter particles with the opposite charge [10].

In contrast to the EM observations, GW observations offer us opportunities to place constraint on the charge of BH in a more robust way. If BHs are indeed highly charged, no matter electric, magnetic, or dark charge, or “charge” in the scalar-tensor-vector gravity [11], they can be described by the Einstein-Maxwell theory and will modify the GW signatures of BBH mergers. As the first step towards constraining the charge of BH with the data of advanced LIGO/Virgo, Wang *et al.* [12] have analyzed

GW data in the first gravitational wave transient catalog (GWTC-1) by assuming that the charge effect can be introduced as perturbation in the inspiral phase of the GW waveform. Recently, by analyzing GW data with numerical relativity (NR) simulations of the coalescence of the charged BBHs, [13] found that GW150914 is compatible with having charge-to-mass ratio of  $\leq 0.3$ . However, these two works mainly focused on the inspiral phase of the GW radiation. Moreover, they are limited by the lack of quadrupole electromagnetic emission [12] and the non-spinning assumption of the black holes of GW150914 [13]. In this work we aim to probe the charge effect with the sole ringdown data.

The QNMs, also called the BH spectroscopies, have been developed to test GR and the no-hair theorem, and to extract the properties of the newly formed BH [14–16]. As shown in Refs. [14, 15], it is efficient and reliable to apply Bayesian analysis to the ringdown spectrum in time domain. Giesler *et al.* [16] found out that the overtone modes play a significant role in ringdown spectrum. For Kerr-Newman (KN) BHs, the QNMs have been studied for many years [10, 17–19]. Particularly, Ref. [19] successfully obtained the spectrum of QNMs of KN BH with numerical calculations, which were limited to the fundamental mode for  $\chi = \lambda$ . Alternatively, the QNMs of BHs in Einstein’s gravity can be related with the null geodesics [20–22], which provides an approximated way to calculate QNMs of BHs. Though derived only in the eikonal limit ( $l \gg 1$ ), such results can be used for qualitative analysis and to make order-of-magnitude estimates [10].

In this work, we calculate both the fundamental and overtone QNMs of the KN BHs by using the (improved) geodesic correspondence method [22] (note that previous ringdown analyses for KN BHs have neglected overtones [10]). Then we compare them with the fundamen-

---

\* Corresponding author: lipch2019@pku.edu.cn.

tal mode given by the NR simulation [19] and the higher modes of the standard Kerr ringdown waveform that is available in LALSUITE software library [23], and the PYCBC package [24]. The validity of our KN model is confirmed by the nice consistency among the results. We also constrain the charge of the remnant of GW150914 to be  $\leq 0.38$  at 90% confidence level. We assume  $G = c = 1$  throughout the paper unless otherwise specified.

## II. METHOD

The computation of the QNMs of the KN BH is very difficult, mainly due to the indissolubility of the coupling between the gravitational perturbations and electromagnetic perturbations [25]. Until now, the exact results are only available in limited cases [17–19]. On the other hand, Ref. [22] shows that the QNM frequency of the Kerr BH in the eikonal limit reads

$$\Omega_{lmn} = \left(l + \frac{1}{2}\right) \left( \Omega_\theta + \frac{m}{l + \frac{1}{2}} \Omega_{prec} \right) - i\alpha\gamma_L \left(n + \frac{1}{2}\right), \quad (1)$$

where  $\Omega_\theta$  is the orbital frequency in the polar direction,  $\Omega_{prec}$  is the Lense-Thirring precession frequency of the orbit plane, and  $\gamma_L$  is the Lyapunov exponent of the orbit, and  $n$  is the overtone number. It was shown in Ref. [22] that the relative error of the result obtained from above formula is not less than 10%, which makes it almost useless for quantitative analysis. However, as a discovery in practice, we find that by replacing the pre-factor  $(l+1/2)$  with  $l$  and  $\alpha = 1$  with  $(l+l^2+l^3)/(1+l+l^2+l^3)$  in Eq. (1), the resulting QNMs match very well with the exact numerical results of both Kerr and KN BHs (we will show it below). Since the explicit expression of the QNM frequency is lengthy we would like to deliver it to the appendix A.

The ringdown waveform of KN BH is fully described by two time-dependent polarizations in GR,  $h(t) = h_+(t) - ih_\times(t)$ , which can be written as

$$h_+(t) - ih_\times(t) = \sum_l \sum_m \sum_n^N A_{lmn} \exp(i(-\Omega_{lmn}t + \phi_{lmn})) \times {}_{-2}Y_{lm}(t), \quad (2)$$

where  $N$  is the total overtone numbers that we considered,  $A_{lmn}, \phi_{lmn}$  characterize the amplitudes and phases of each ringdown mode at the peak,  $\iota$  is the inclination angle, and  ${}_{-2}Y_m(t)$  are the spin-weighted spherical harmonics. The response of a single detector  $k$  to the GWs can be described as

$$h_k(t) = F_k^+(\alpha, \delta, \psi)h_+(t) + F_k^\times(\alpha, \delta, \psi)h_\times(t), \quad (3)$$

where  $F_k^{+, \times}(\alpha, \delta, \psi)$  are the antenna beam patterns,  $\alpha, \delta$  are the right ascension and declination angles, and  $\psi$  is the polarization angle.

The GW data stream  $d$  is provided by the Gravitational-Wave Open Science Center [26], which contains the signal  $h(t)$  and noise  $n(t)$ . In standard GW data analysis, the detector noise can be assumed to be a Gaussian stochastic process, which has been well checked already [27]. A Gaussian stochastic process is one for which each set  $[n(t_0), n(t_1), \dots, n(t_{N_s-1})]$  is distributed as multivariate Gaussian probability density function (PDF),

$$\mathbf{n}(t) \sim \mathcal{N}(\boldsymbol{\mu}, \boldsymbol{\Sigma}), \quad (4)$$

where  $\boldsymbol{\mu}$  and  $\boldsymbol{\Sigma}_{ij} = \rho(i-j)$  are the mean and the covariance matrix of the noise time series, respectively. After applying a high-pass filter with a roll-on frequency of 20 Hz, the data stream can be treated as zero mean.  $\rho$  is the autocovariance function,

$$\rho(i-j) = \langle n_i n_j \rangle, \quad (5)$$

and  $\rho(-n) = \rho(N_s - n)$  for  $0 \leq n < N_s$ , where  $N_s$  is the total number of samples. According to the Wiener-Khinchin theorem, the autocovariance function is the inverse Fourier transform of the power spectral density (PSD). In our case, the covariance matrix is special as a circulant Toeplitz matrix, therefore the inverse of it can be simply solved with SCIPY package [28].

For GW data analysis in time domain, the inner product between two waveforms  $h_1(t)$  and  $h_2(t)$  can be defined as

$$(h_1 | h_2) = h_1^T \boldsymbol{\Sigma}^{-1} h_2. \quad (6)$$

To quantify the mismatch between two waveforms  $h_1, h_2$ , we define it as

$$\begin{aligned} \text{Mismatch} &= 1 - \mathcal{O}(h_1, h_2) \\ &= 1 - \frac{(h_1 | h_2)}{\sqrt{(h_1 | h_1)(h_2 | h_2)}}. \end{aligned} \quad (7)$$

Obviously, the value of Mismatch approaches to 0 if these two waveforms match well with each other.

Given the presence of the observed strain series  $d_k(t)$  and the GW signal  $h_k(t)$  from waveform model, the log-likelihood function can be written as

$$\log \mathcal{L}_k = -\frac{1}{2}(d_k - h_k | d_k - h_k). \quad (8)$$

Then the log-likelihood function of multiple detectors is the sum of the individual log-likelihood.

For GW150914, the ringdown signal in the GW data is shorter than 0.02 seconds [27]. In this work, the Bayesian analyses are performed with 4 seconds data stream that around the peak. In addition to the fundamental mode  $(2, 2, 0)$ , we also consider the first overtone mode  $(2, 2, 1)$  in our analyses. As pointed out by the studies in Refs. [15, 16], these two modes are sufficient for the ringdown analysis.

To estimate the parameters with the ringdown signal of GW150914, we carry out Bayesian inference with BILBY

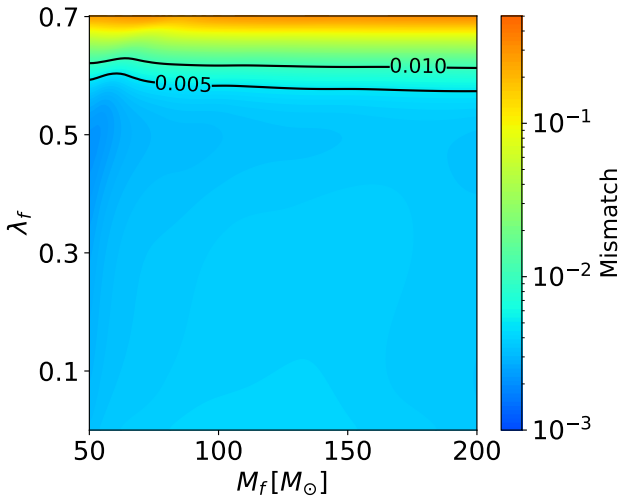


FIG. 1. Distribution of mismatch over final charge and final mass, assuming that  $\lambda_f = \chi_f$ . The black lines represent contours on the mismatch between NR waveform and our KN waveform.

package [29] and DYNESTY sampler [30]. Following Isi et al. [15], we fix some extrinsic parameters in our analyses: the geocentric time is set to be 1126259462.408 GPS, the right ascension is  $\alpha = 1.95$  rad, the declination is  $\delta = -1.27$  rad, the polarization angle is  $\psi = 0.82$  rad, and the inclination angle is  $\iota = \pi$  rad. Meanwhile, the parameters above are also fixed when we make waveform comparison. The priors on the final mass  $M_f$ , the dimensionless spin  $\chi_f$ , the amplitudes parameter  $A_{lmn}$ , and the phase parameter  $\phi_{lmn}$  are uniformly distributed in the ranges of  $[50, 100]M_\odot$ ,  $[0, 0.99]$ ,  $[0, 5]$ , and  $[0, 2\pi]$ , respectively. For the dimensionless charge  $\lambda_f$  in the ringdown waveform of KN BH, the prior is uniform in the range of  $[0, 1]$ . Additionally, there is a constraint on  $\lambda_f$  and  $\chi_f$ ,  $\lambda_f^2 + \chi_f^2 \leq 1$ , which comes from the avoidance of the appearance of a naked singularity.

### III. RESULTS

First and foremost, we compare our KN ringdown waveform with the previous works by considering a single detector of LIGO with the design sensitivity to check whether it can be applied to GW data analysis. We first compare our waveform with the KN ringdown waveform in Ref. [19], which offers the data of the fundamental mode limited to the case of  $\lambda_f = \chi_f$ . And in this case, the maximum value of the final charge is  $\lambda_f = \chi_f \approx 0.7$ , which is due to the theoretic constraint mentioned above. We use the mismatch defined in Eq. (7) to investigate whether these two KN ringdown waveform models are indistinguishable. Since we only focus on  $(M_f, \lambda_f, \chi_f)$  among parameters of  $(M_f, \lambda_f, \chi_f, A_{220}, \phi_{220})$  here, we assume  $A_{220} = 0.6$ ,  $\phi_{220} = 0$ ,  $\lambda_f = \chi_f$  and calculate the mismatches with  $M_f$  lying in the range of  $[50, 200]M_\odot$

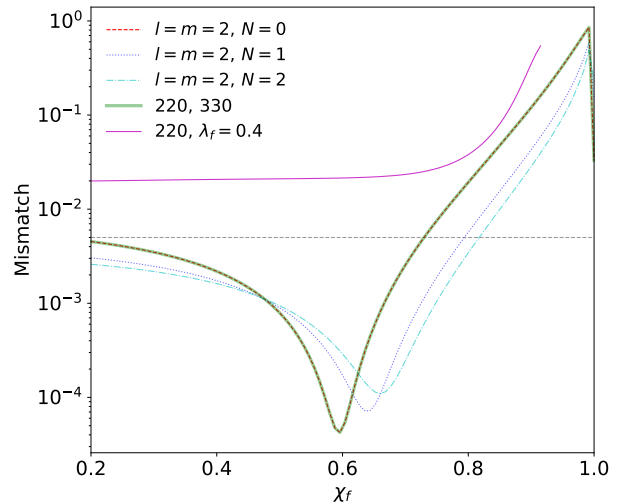


FIG. 2. Mismatch ranges over  $\chi_f$ , assuming  $M_f = 100M_\odot$ . The horizontal dashed gray line marks the mismatch at 0.005. We consider the fundamental mode with zero overtone (dashed red), one overtone (dotted blue), two overtones (dash dotted cyan), and higher mode  $l = m = 3$  (bold green). The purple curve represents a special case that  $\lambda_f = 0.4$  for fundamental mode in KN ringdown waveform, while other parameters are the same as that in standard Kerr waveform. These two ringdown waveform models match better when more overtones are included.

and  $\lambda_f = \chi_f$  in the range of  $[0, 0.7]$ .

For a signal with signal-to-noise ratio (SNR)  $\rho$ , the mismatch should be smaller than  $1/(2\rho^2)$  if two waveform models match well with each other [31, 32]. The SNR of single detector for the ringdown stage of GW150914 is about 10 [15], which means that the mismatch threshold is 0.005. Compared with the realistic PSD, the PSD of design sensitivity for LIGO could increase the mismatch between two different waveforms, so 0.005 is a conservative choice in our analysis. As shown in Fig. 1, the mismatch keeps unchanged when  $M_f$  ranged from  $50M_\odot$  to  $200M_\odot$ . When  $\lambda_f = \chi_f \leq 0.63$ , the mismatch is smaller than 0.01, and if  $\lambda_f = \chi_f \leq 0.60$ , it is smaller than the threshold value 0.005. This result indicates that the difference of the fundamental mode between these two waveform models is acceptable in GW data analysis currently. <sup>1</sup>

However, the comparison above can not be made, since there is no available KN ringdown waveform for  $N > 1$  case up to now. Alternatively, by setting  $\lambda_f = 0$  in our KN ringdown waveform we can make comparison with the standard Kerr ringdown waveform used in Refs. [15, 16]. In this case, we assume  $M_f = 100M_\odot$

<sup>1</sup> A similar analysis for the mismatch of the  $(2, 2, 0)$  mode based weakly charged KN waveform [10, 18] can be found in Ref. [33].

since it has little influence on the mismatch. The amplitudes  $A_{lmn}$  and phases  $\phi_{lmn}$  are also fixed to  $A_{221} = 1.2, A_{222} = 0.8, A_{330} = 1, \phi_{221} = \phi_{222} = \phi_{330} = 0$ . The final spin ranges from 0 to 0.998 while other parameters are the same as analysis above. It is noticeable that our ringdown waveform behaves better if more overtone modes are included (as shown in Fig. 2). When the final spin is smaller than 0.8, the mismatch is smaller than 0.005 if  $N \geq 1$ . Fortunately, the final spins of almost all GW events are smaller than 0.8, as shown in TABLE VIII of [34]. We also find that the 330 mode has little contribution compared with the 220 mode, which is consistent with the study in Ref. [14]. Specially, we compute the mismatch between the KN ringdown waveform ( $\lambda_f = 0.4$ ) and the standard Kerr waveform (other parameters are the same for both waveforms). Compared with the  $\lambda_f = 0$  case (dashed red curve in Fig. 2), the mismatch of  $\lambda_f = 0.4$  case drops about 2% when  $\chi_f \leq 0.8$ . This means that  $\lambda_f = 0.4$  leads to a detectable difference for KN ringdown waveform model.

From the analysis above, it can be confirmed that our KN ringdown waveform behaves well for the fundamental mode. The cases of  $N > 0$  have also been carefully checked by comparing them with the standard Kerr ringdown waveform. Furthermore, one can reduce the mismatch by including more overtones when performing GW data analysis.

Using the posteriors of GW150914 (IMRPhenomPv2 case) released by LVC [26], we translate them into the posteriors of final mass and final spin in detector frame. Then we perform Bayesian analysis with the ringdown signal of GW150914, using standard Kerr ringdown waveform and our KN ringdown waveform. For the standard Kerr ringdown waveform model, we obtain similar results compared to Ref. [15]. For comparison, we set  $\lambda = 0$  for KN ringdown waveform to quantify the difference between it and the standard Kerr ringdown waveform model. As shown in Fig. 3, the 90%-credible region of IMRPhenomPv2 model is well covered by both of these two models. If we set  $\lambda \neq 0$ , the distribution is similar to  $\lambda = 0$ , which means that there is no strong evidence that GW150914 is strongly charged. The posterior distribution of  $\lambda_f$  obtained by analyzing GW150914 with KN ringdown waveform is shown in Fig. 4. Apparently, the distribution of  $\lambda_f$  can approach 0 which is consistent with Kerr BH case.

And the constraint on  $\lambda_f$  is obtain as  $\lambda_f \leq 0.38$  at 90% confidence level, which is comparable with the constraint of  $\lambda_f \leq 0.3$  given by Ref. [13] under assumption that only one BH in GW150914 is charged. Strictly speaking, our methods are more flexible since we perform our analysis with Bayesian inference. While Bozzola and Paschalidis [13] obtained their results by fixing all other parameters of GW waveform, which mainly due to the numerous computation in NR simulation. Note that what we constrain here is the final charge of GW150914, which is different from the constraint in Ref. [13]. And this constraint means that  $\lambda_f = 0.4$  leads to a detectable differ-

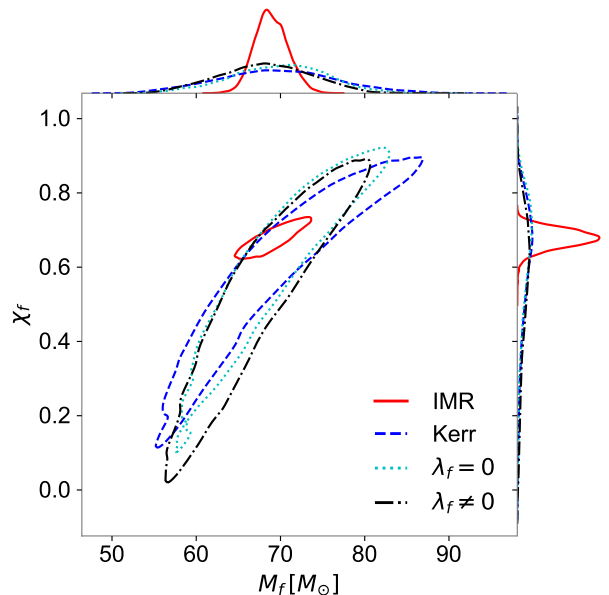


FIG. 3. Posterior distributions of final mass and final spin for GW150914. All of the contours are 90%-credible regions. The 1D marginalized posterior distributions for final mass and final spin are shown in the top and right-hand panels respectively. The red solid contour represents the result of using IMRPhenomPv2 model [35], published by LIGO-Virgo collaboration (LVC) [26]. The analysis using standard Kerr ringdown waveform is represented by dashed blue contour. For KN ringdown waveform model, the distributions are similar for both  $\lambda = 0$  (dotted green) and  $\lambda \neq 0$  (dash dotted black).

ence for KN ringdown waveform, which agrees with the analysis shown in Fig. 2.

#### IV. SUMMARY

In this work, we computed the QNMs of the KN black holes through the geodesic correspondence method [22] and obtained the KN ringdown waveform consisting of the fundamental and overtone QMNs. Then we compared our KN ringdown waveform with other waveforms using the mismatch defined in Eq. (7). The mismatch between these two waveform modes, insensitive on the final mass, is smaller than 0.005 for  $\lambda_f = \chi_f \leq 0.60$ . For astrophysical BHs, the charges can hardly reach 0.60, so our KN waveform model is feasible in GW data analysis. Notice that the contribution of overtone, which is significant in ringdown-only analysis [15, 16], is excluded in the comparison above. So we compare our KN ringdown waveform with the standard Kerr ringdown waveform [15, 16]. The consistence is remarkable. Assuming a  $\lambda = 0.4$  in KN ringdown waveform, the effect is detectable for advanced LIGO.

We also perform Bayesian analyses with both the

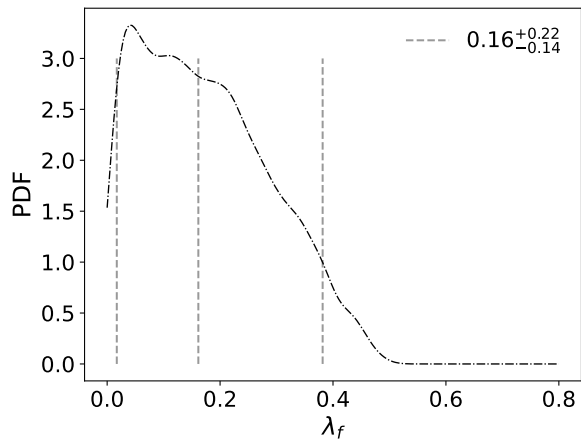


FIG. 4. Posterior distribution of  $\lambda_f$  obtained by analyzing GW150914 with KN ringdown waveform. The dashed vertical gray lines represent the median value and 90%-credible measurement of  $\lambda_f$ , and their values are shown in the upper right.

KN ringdown waveform and the standard Kerr ringdown waveform. The posterior distributions of the final mass/spin of these two waveform models are nicely in agreement with the results from IMRPhenomPv2 model. For GW150914, the final charge of the remnant BH is constrained to be smaller than 0.38 (at 90% credible level). It is also straightforward to extend our analysis to other events that are suitable for ringdown-only analyses [34].

Finally, similar to Ref. [13], since our approach is based on the Einstein-Maxwell theory and the KN metric, it can be directly applied to black holes endowed with hidden or dark charges [10], and black holes carried with magnetic charge through the electromagnetic duality. Moreover,

the constraint on the final charge we obtained in this work can also be translated to the constraint on the deviation parameter of the scalar-tensor-vector gravity [11] by the relation  $\lambda_f = \sqrt{\alpha/(1+\alpha)}$ . The  $\lambda_f \leq 0.38$  found in GW150914 yields that  $\alpha \leq 0.17$ , which is the first constraint on the scalar-tensor-vector gravity with the sole ringdown data.

## ACKNOWLEDGMENTS

H. T. W. also appreciates M. Z. H. and J. L. J. for insightful comments and discussions. This work has been supported by NSFC under grants of No. 11921003, No. 11847241, No. 11947210 and No. 12047550. PCL is also funded by China Postdoctoral Science Foundation Grant No. 2020M670010. This research has made use of data, software and/or web tools obtained from the Gravitational Wave Open Science Center (<https://www.gwopenscience.org>), a service of LIGO Laboratory, the LIGO Scientific Collaboration and the Virgo Collaboration. LIGO is funded by the U.S. National Science Foundation. Virgo is funded by the French Centre National de Recherche Scientifique (CNRS), the Italian Istituto Nazionale della Fisica Nucleare (INFN) and the Dutch Nikhef, with contributions by Polish and Hungarian institutes.

## Appendix A: Explicit expression of the QNM frequency

Using the formula provided by [22] and [10], the explicit expression of the QNM frequency for  $l = m$  is given by

$$\begin{aligned} \Omega_{ltn} = & \frac{M\chi l}{r^2(2l+1)(r(2\lambda^2 M^2 - 3Mr + r^2) + M^2\chi^2(M+r))} \left[ 2Mr^2 l - 2r^3 l \right. \\ & \left. + \sqrt{M^2(\lambda^2 + \chi^2) - 2Mr + r^2} \sqrt{-4\lambda^2 M^4(\lambda^2 + \chi^2) + 8M^3 r(2\lambda^2 + \chi^2) - (4\lambda^2 + 15)M^2 r^2 + 6Mr^3 + r^4} \right] \\ & - \frac{i\alpha M^{3/2}(2n+1)r^2\chi\sqrt{3r - 4\lambda^2 M}(M^2(\lambda^2 + \chi^2) - 2Mr + r^2)}{r^4(r(2\lambda^2 M^2 - 3Mr + r^2) + M^2\chi^2(M+r))}, \end{aligned} \quad (\text{A1})$$

where

$$\begin{aligned} r = & 2M(\cos\phi + 1) - \frac{\lambda^2 M(\chi^2 + 2\cos(\phi) + 2\cos(2\phi))}{3(\chi^2 + \cos(\phi) + \cos(2\phi))} \\ & + \frac{\lambda^4 M}{36(\chi^2 + \cos(\phi) + \cos(2\phi))^3} \left[ -5\chi^4 + 32\chi^2 - 4(3\chi^4 - 4\chi^2 - 3)\cos(\phi) - 4 \right. \\ & \left. 8\chi^2\cos(4\phi) + 4(\chi^4 + 2\chi^2 + 3)\cos(2\phi) + 4\cos(4\phi) + 4\cos(5\phi) + 4\cos(6\phi) \right] + \mathcal{O}(\lambda^6), \end{aligned} \quad (\text{A2})$$

with

$$\phi = \frac{2}{3} \cos^{-1}(-\chi). \quad (\text{A3})$$

- 
- [1] C. V. Vishveshwara, *Phys. Rev. D* **1**, 2870 (1970).
- [2] W. H. Press, *Astrophysical Journal, Letters* **170**, L105 (1971).
- [3] S. A. Teukolsky, *Astrophysical Journal* **185**, 635 (1973).
- [4] B. Carter, *Phys. Rev. Lett.* **26**, 331 (1971).
- [5] W. Israel, *Phys. Rev.* **164**, 1776 (1967).
- [6] W. Israel, *Commun. Math. Phys.* **8**, 245 (1968).
- [7] V. Cardoso and L. Gualtieri, *Classical and Quantum Gravity* **33**, 174001 (2016).
- [8] A. F. Zakharov, *Phys. Rev. D* **90**, 062007 (2014).
- [9] M. Zajaček, A. Tursunov, A. Eckart, S. Britzen, E. Hackmann, V. Karas, Z. Stuchlík, B. Czerny, and J. A. Zensus, *Journal of Physics: Conference Series* **1258**, 012031 (2019).
- [10] V. Cardoso, C. F. B. Macedo, P. Pani, and V. Ferrari, *Journal of Cosmology and Astroparticle Physics* **2016**, 054 (2016), [arXiv:1604.07845 \[hep-ph\]](#).
- [11] J. W. Moffat, *JCAP* **03**, 004 (2006), [arXiv:gr-qc/0506021](#).
- [12] H.-T. Wang, P.-C. Li, J.-L. Jiang, Y.-M. Hu, and Y.-Z. Fan, *arXiv e-prints*, [arXiv:2004.12421](#) (2020), [arXiv:2004.12421 \[gr-qc\]](#).
- [13] G. Bozzola and V. Paschalidis, *Phys. Rev. Lett* **126**, 041103 (2021), [arXiv:2006.15764 \[gr-qc\]](#).
- [14] G. Carullo, W. Del Pozzo, and J. Veitch, *Phys. Rev. D* **99**, 123029 (2019).
- [15] M. Isi, M. Giesler, W. M. Farr, M. A. Scheel, and S. A. Teukolsky, *Phys. Rev. Lett.* **123**, 111102 (2019).
- [16] M. Giesler, M. Isi, M. A. Scheel, and S. A. Teukolsky, *Physical Review X* **9**, 041060 (2019), [arXiv:1903.08284 \[gr-qc\]](#).
- [17] P. Pani, E. Berti, and L. Gualtieri, *Phys. Rev. Lett* **110**, 241103 (2013), [arXiv:1304.1160 \[gr-qc\]](#).
- [18] Z. Mark, H. Yang, A. Zimmerman, and Y. Chen, *Phys. Rev. D* **91**, 044025 (2015), [arXiv:1409.5800 \[gr-qc\]](#).
- [19] Ó. J. C. Dias, M. Godazgar, and J. E. Santos, *Phys. Rev. Lett* **114**, 151101 (2015), [arXiv:1501.04625 \[gr-qc\]](#).
- [20] V. Ferrari and B. Mashhoon, *Phys. Rev. D* **30**, 295 (1984).
- [21] V. Cardoso, A. S. Miranda, E. Berti, H. Witek, and V. T. Zanchin, *Phys. Rev. D* **79**, 064016 (2009), [arXiv:0812.1806 \[hep-th\]](#).
- [22] H. Yang, D. A. Nichols, F. Zhang, A. Zimmerman, Z. Zhang, and Y. Chen, *Phys. Rev. D* **86**, 104006 (2012), [arXiv:1207.4253 \[gr-qc\]](#).
- [23] LIGO Scientific Collaboration, “LIGO Algorithm Library - LALSuite,” free software (GPL) (2018).
- [24] C. M. Biwer, C. D. Capano, S. De, M. Cabero, D. A. Brown, A. H. Nitz, and V. Raymond, *PASP* **131**, 024503 (2019), [arXiv:1807.10312 \[astro-ph.IM\]](#).
- [25] S. Chandrasekhar, *The mathematical theory of black holes* (1985).
- [26] B. P. Abbott, R. Abbott, and T. D. e. a. Abbott (LIGO Scientific Collaboration and Virgo Collaboration), *Phys. Rev. X* **9**, 031040 (2019).
- [27] B. P. Abbott, R. Abbott, and T. D. e. a. Abbott (LIGO Scientific Collaboration and Virgo Collaboration), *Phys. Rev. Lett.* **116**, 061102 (2016).
- [28] E. Jones, T. Oliphant, and P. Peterson, (2001).
- [29] G. Ashton, M. Hübner, P. D. Lasky, C. Talbot, K. Ackley, S. Biscoveanu, Q. Chu, A. Divakarla, P. J. Easter, B. Goncharov, F. H. Vivanco, J. Harms, M. E. Lower, G. D. Meadors, D. Melchor, E. Payne, M. D. Pitkin, J. Powell, N. Sarin, R. J. E. Smith, and E. Thrane, *The Astrophysical Journal Supplement Series* **241**, 27 (2019).
- [30] J. S. Speagle, *MNRAS* **493**, 3132 (2020), [arXiv:1904.02180 \[astro-ph.IM\]](#).
- [31] É. É. Flanagan and S. A. Hughes, *Phys. Rev. D* **57**, 4566 (1998), [arXiv:gr-qc/9710129 \[gr-qc\]](#).
- [32] L. Lindblom, B. J. Owen, and D. A. Brown, *Phys. Rev. D* **78**, 124020 (2008), [arXiv:0809.3844 \[gr-qc\]](#).
- [33] G. Bozzola and V. Paschalidis, (2021), [arXiv:2104.06978 \[gr-qc\]](#).
- [34] B. P. Abbott, R. Abbott, and T. D. e. a. Abbott, *arXiv e-prints*, [arXiv:2010.14529](#) (2020), [arXiv:2010.14529 \[gr-qc\]](#).
- [35] M. Hannam, P. Schmidt, A. Bohé, L. Haegel, S. Husa, F. Ohme, G. Pratten, and M. Pürrer, *Phys. Rev. Lett.* **113**, 151101 (2014).